Analytical Solutions to a Rijke Tube System with Periodic Excitations through a Semi-Analytical Approach

Jianzhe Huang

Shanghai Jiao Tong University, Shanghai 200240

E-mail: huangdeng9@sjtu.edu.cn

Abstract: Thermoacoustic instability problems are widely existed in many real world applications such as gas turbines, rocket motors etc. A Rijke tube is a typical thermoacoustic system, and it is difficult to analyze such a system due to the nonlinearity and time delay. In this paper, a set of nonlinear ordinary differential equations with time delay which represent a Rijke tube system will be studied. The state space of such a tube system is consisted of velocity and pressure, and the periodic motion can be discretized based on an implicit mid-point scheme. Through Newton-Raphson method, the node points on the periodic motion will be solved, and the analytical solution of such a periodic motion for Rijke tube system can be recovered using a set of Fourier representations. According to the theory of discrete maps, the stability of the periodic motion will be obtained. Finally, specific system parameters will be adopted in order to carry out numerical studies to show different periodic motions for such a tube system. The analytical bifurcations which show how period-1 motion involves to period-m motion and then becomes chaos will be demonstrated. With such a technique, some interesting nonlinear phenomenon will be explained analytically, which will be of great help to understand and control such a Rijke tube system.

Key Words: Thermoacoustic, Periodic Motions, Chaos, Semi-Analytic, Bifurcation

1. Introduction

In the 1800s, Rijke [1] found that an open-ended vertical tube could produce loud sound by placing hot metal gauze in the lower half, and such a tube is now named as Rijke tube. But he did not explain why hot gauze in the upper half of the tube did not produce sound. Rayleigh [2] explained the phenomena observed by Rijke, and a criterion was proposed for the development of heat-driven oscillations. For vertical Rijke tube, it is difficult to use for quantitative testing due to the acoustic coupling. In 1964, Friedlander et al. [3] studied the horizontal Rijke tube, and the sound pressure level varying with relative heater position for different tube length was discussed experimentally. Bisio and Rubatto [4] designed a feedback control system to achieve the active control of noise for a horizontal Rijke tube. In 2008, Balasubramanian and Rujith [5] modeled the heat release rate of the heating

element for Rijke tube using a modified form of King's law, and algebraic growth of oscillations was induced by the non-normality of the thermoacousitc system. For horizontal Rijke tube, the governing equations for the fluid flow are too stiff to be solved through computational fluid dynamics due to the small Mach number of the steady flow and the small thickness of the heat source. The numerical model for horizontal Rijke tube was proposed in [6]. Then Mariappan and Sujith [7] used Galerkin method to simulate the acoustic zone and CFD technique to model the hydrodynamic zone. It showed that the bifurcation results were different with and without the global-acceleration term. Juniper et al. [8] studied a horizontal Rijke tube model with radius of the upstream and downstream ducts varied, the perturbation method was adopted to obtain the solutions of such a system and weakly nonlinear analysis has been carried out. For such a Rijke tube system with strong nonlinearity, it is difficult to calculate the solution analytically since traditional analytic methods for nonlinear system are only valid for weak nonlinear problems. Generalized harmonic balance method [9] is an ideal tool for getting the approximate solutions which correlate with numerical simulation very well for strong nonlinear systems, and it can also deal with nonlinear dynamical system with time-delayed term [10]. However, it will take a great effort to derive the equations for such a Rijke tube model, since the degrees of freedom could be high when more mode shapes have been included [11]. The discrete implicit maps method [12] is a newly developed technology for solving various dynamical systems with strange nonlinear terms. With such a method, Wang and Huang [13] gave an analytical solution for periodic motions for a damped mobile piston system in a high pressure gas cylinder with P control, and there was no computational error to calculate the bifurcation points since the dimension of the Jocobian matrix did not increase with the truncated order of harmonics for periodic solution increases. Guo and Luo [14] adopted the discrete implicit maps method to investigate the parametrically driven pendulum for which the nonlinear term is a triangular function, and the complex bifurcation diagrams of analytic solutions for periodic motions were presented. For time-delayed systems, Luo and Xing [15] studied the periodically forced hardening Duffing oscillator with time delay through the discrete implicit method, and the time-delay effects on period-1 to chaos for such a dynamical system have been discussed.

In this paper, a horizontal Rijke tube with periodical acoustic source will be studied. The acoustic momentum and energy equations for such a Rijke tube will be converted into a set of ordinary differential equations through Galerkin transformation. The time-delayed effect will be introduced due to the heat release rate fluctuations of the heat source for such a horizontal Rijke tube. The periodic motion will be discretized into a finite number of node points with constant time interval, and one node point maps to another one based on implicit midpoint scheme. The time-delayed term will be represented by the normal states due to the periodicity, and the node points can be solved through Newton-Raphson method. From the node points, the analytic solution of periodic motion will be recovered using a set of finite Fourier series. Then the harmonic amplitudes varying amplitude of periodic acoustic excitation will be illustrated. Some numerical simulations will be given to discuss the dynamic behaviors of such a horizontal Rijke tube with periodical acoustic source.

2. Model and Semi-Analytic Method

For a horizontal Rjike tube, the governing equations can be given in Eqs. (1) and (2) by assuming that the system is symmetric, Mach number of the mean flow is small, and a perfect open-open acoustic boundary condition at both ends of the tube.

$$\gamma M \frac{\partial u'}{\partial t} + \frac{\partial p'}{\partial x} = 0 \tag{1}$$

$$\frac{\partial p'}{\partial t} + \gamma M \frac{\partial u'}{\partial x} + \zeta p' = \frac{\gamma MK}{2}\left(\sqrt{\left|\frac{1}{3} + u_f'(t-\tau)\right|} - \frac{1}{3}\right)\delta(x - x_f) \tag{2}$$

where u' and p' are the non-dimensional acoustic velocity and pressure, respectively; x is the non-dimensional axial distance measured from the inlet; t is the non-dimensional time; M is the Mach number of the steady state flow; γ is the adiabatic index; ζ is the damping coefficient; K is the non-dimensional heater power. The subscript *f* means the position of heater inside the Rijke tube. Therefore, the Dirac delta function at the right-hand-side of Eq. (2) indicates that the heat effect only exists at the location of the heater.

Represent velocity and pressure by Fourier series, and it gives

$$u' = \sum_{i=1}^{N} \cos(i\pi x) U_i(t) \tag{3}$$

$$p' = \gamma M \sum_{i=1}^{N} \sin(i\pi x) P_i(t) \tag{4}$$

Then substitute Eqs. (3) and (4) into Eqs. (1) and (2), and perform the Galerkin transform. Then the aforementioned partial differential equations becomes

$$\dot{U}_i + i\pi P_i = 0 \tag{5}$$

$$\dot{P}_i - i\pi U_i + \zeta P_i = K\left(\sqrt{\left|\frac{1}{3} + u_f'(t-\tau)\right|} - \frac{1}{3}\right)\sin(i\pi x_f) \tag{6}$$

In Ref. [16], the damping coefficient ζ for i^{th} mode is expressed as

$$\zeta = \zeta_i = c_1 i^2 + c_2\sqrt{i} \tag{7}$$

Then Eq. (6) can be rewritten as

$$\dot{P}_i - i\pi U_i + \zeta_i P_i = K\left(\sqrt{\left|\frac{1}{3} + u_f'(t-\tau)\right|} - \frac{1}{3}\right)\sin(i\pi x_f) \tag{8}$$

Introduce a periodic excitation into the system, equation (8) then becomes

$$\dot{P}_i - i\pi U_i + \zeta_i P_i = K\left(\sqrt{\left|\frac{1}{3} + u_f'(t-\tau)\right|} - \frac{1}{3}\right)\sin(i\pi x_f) + Q_i \sin(\Omega t) \tag{9}$$

Define $\mathbf{x} \equiv \{U_1, U_2, ..., U_N\}^T$ and $\mathbf{y} \equiv \{P_1, P_2, ..., P_N\}^T$, then Eqs. (5) and (9) can be written in the matrix form as

$$\dot{\mathbf{x}} = \begin{bmatrix} \dot{U}_1 \\ \dot{U}_2 \\ \vdots \\ \dot{U}_N \end{bmatrix} = \begin{bmatrix} -\pi P_1 \\ -2\pi P_1 \\ \vdots \\ -N\pi P_N \end{bmatrix} = -\mathbf{k}\mathbf{y} \tag{10}$$

$$\begin{aligned} \dot{\mathbf{y}} = \begin{bmatrix} \dot{P}_1 \\ \dot{P}_2 \\ \vdots \\ \dot{P}_N \end{bmatrix} &= \begin{bmatrix} -\zeta_1 P_1 + \pi U_1 \\ -\zeta_2 P_2 + 2\pi U_2 \\ \vdots \\ -\zeta_N P_1 + N\pi U_1 \end{bmatrix} + K\left(\sqrt{\left|\frac{1}{3} + u_f'(t-\tau)\right|} - \sqrt{\frac{1}{3}}\right)\begin{bmatrix} \sin\pi x_f \\ \sin 2\pi x_f \\ \vdots \\ \sin N\pi x_f \end{bmatrix} \\ &= -\mathbf{c}\mathbf{y} + \mathbf{k}\mathbf{x} + K\left(\sqrt{\left|\frac{1}{3} + u_f'(t-\tau)\right|} - \sqrt{\frac{1}{3}}\right)\mathbf{f}_1 \end{aligned} \tag{11}$$

where

$$\mathbf{k}=\begin{bmatrix} \pi & 0 & 0 & \cdots & 0 \\ 0 & 2\pi & 0 & \cdots & \vdots \\ 0 & 0 & \ddots & \vdots & 0 \\ \vdots & \cdots & 0 & (N-1)\pi & 0 \\ 0 & \cdots & 0 & 0 & N\pi \end{bmatrix}$$

$$\mathbf{c}=\begin{bmatrix} \zeta_1 & 0 & 0 & \cdots & 0 \\ 0 & \zeta_2 & 0 & \cdots & \vdots \\ 0 & 0 & \ddots & \vdots & 0 \\ \vdots & \cdots & 0 & \zeta_{N-1} & 0 \\ 0 & \cdots & 0 & 0 & \zeta_N \end{bmatrix}$$

$$\mathbf{f}_1=\begin{bmatrix} \sin\pi x_f & \sin 2\pi x_f & \cdots & \sin N\pi x_f \end{bmatrix}^T$$

For a period-*m* motion of such a horizontal Rijke tube, the trajectory is discretized into *mL* partitions. The mapping P_k (k = 0, 1,…, *mL*-1), which maps from one node point with state vector $(\mathbf{x}_k, \mathbf{y}_k, \mathbf{x}_{k-\mathrm{int}(\tau/h)-1}, \mathbf{x}_{k-\mathrm{int}(\tau/h)}, \mathbf{x}_{k-\mathrm{int}(\tau/h)+1})$ to another node point with state vector $(\mathbf{x}_{k+1}, \mathbf{y}_{k+1}, \mathbf{x}_{k-\mathrm{int}(\tau/h)}, \mathbf{x}_{k-\mathrm{int}(\tau/h)+1}, \mathbf{x}_{k-\mathrm{int}(\tau/h)+2})$, is expressed by

$$\mathbf{x}_{k+1}=\mathbf{x}_k-\frac{1}{2}h\mathbf{k}(\mathbf{y}_k+\mathbf{y}_{k+1}) \tag{12}$$

$$\mathbf{y}_{k+1}=\mathbf{y}_k+h\left[-\mathbf{c}\frac{\mathbf{y}_k+\mathbf{y}_{k+1}}{2}+\mathbf{k}\frac{\mathbf{x}_k+\mathbf{x}_{k+1}}{2}+K\left(\sqrt{\left|\frac{1}{3}+V\right|}-\sqrt{\frac{1}{3}}\right)\mathbf{f}_1+\mathbf{Q}\sin\Omega(t_k+\frac{h}{2})\right] \tag{13}$$

where

$$V=\frac{1}{2}\left[u_f'(t_k-\tau)+u_f'(t_{k+1}-\tau)\right] \tag{14}$$

$$u_f'(t_k-\tau)=\left\{\mathbf{x}^T_{k-\mathrm{int}(\tau/h)-1}+\left[1-\frac{\tau}{h}+\mathrm{int}\left(\frac{\tau}{h}\right)\right]\left(\mathbf{x}^T_{k-\mathrm{int}(\tau/h)}-\mathbf{x}^T_{k-\mathrm{int}(\tau/h)-1}\right)\right\}\mathbf{f}_2 \tag{15}$$

$$\mathbf{Q}=\begin{bmatrix} Q_1, Q_2, ..., Q_N \end{bmatrix}^T$$

and where

$$\mathbf{f}_2=\begin{bmatrix} \cos\pi x_f & \cos 2\pi x_f & \cdots & \cos N\pi x_f \end{bmatrix}^T$$

$$\mathbf{x}_k \equiv \mathbf{x}(t = t_k), \quad \mathbf{y}_k \equiv \mathbf{y}(t = t_k) \quad \text{and} \quad h = 2\pi / (L\Omega).$$

Due to the periodicity, it has $\mathbf{x}_0 = \mathbf{x}_{mL}$ and $\mathbf{y}_0 = \mathbf{y}_{mL}$. Categorize the node points into a single set, one have

$$\mathbf{z} \equiv \{\mathbf{x}_0, \mathbf{y}_0, \mathbf{x}_1, \mathbf{y}_1, \cdots, \mathbf{x}_{mL-1}, \mathbf{y}_{mL-1}\}^T \tag{16}$$

To solve those node points **z**, one gives the initial approximations **z***. Rearrange Eqs. (12) and (13), and it gives

$$\mathbf{g}_{1k} = -\mathbf{x}_{k+1} + \mathbf{x}_k - \frac{1}{2} h\mathbf{k}(\mathbf{y}_{k+1} + \mathbf{y}_k) \tag{17}$$

$$\mathbf{g}_{2k} = -\mathbf{y}_{k+1} + \mathbf{y}_k + h\left[-\mathbf{c}\frac{\mathbf{y}_k + \mathbf{y}_{k+1}}{2} + \mathbf{k}\frac{\mathbf{x}_k + \mathbf{x}_{k+1}}{2} + K\left(\sqrt{\left|\frac{1}{3} + V\right|} - \sqrt{\frac{1}{3}}\right)\mathbf{f}_1 + \mathbf{Q}\sin\Omega(t_k + \frac{h}{2}) \right] \tag{18}$$

Define $\mathbf{g} \equiv \{\mathbf{g}_{10}, \mathbf{g}_{20}, \mathbf{g}_{11}, \mathbf{g}_{21}, \cdots, \mathbf{g}_{1L}, \mathbf{g}_{2L}\}^T$, and put such initial approximates into Eqs. (17) and (18) to calculate **g*** for the first iteration. According to Newton-Raphson algorithm, the increment of the approximations for the next iteration can be obtained as

$$\left[\frac{\partial \mathbf{g}}{\partial \mathbf{z}}\right]\Big|_{\mathbf{z}=\mathbf{z}^*} \Delta\mathbf{z} = \mathbf{g}^* \tag{19}$$

Then the approximates for the next iteration can be obtained as **z**** = **z*** + Δ**z**, and the iteration terminates until $\|\Delta\mathbf{z}\| < \varepsilon$ where ε is the preset convergence criterion.

For the k^{th} node point, the velocity $u_f'(t_k)$ and pressure $u_f'(t_k)$ at the position of heater can be computed with Eqs. (3) and (4). The analytic solution of velocity and pressure at the position of heater for period-m motion for such a horizontal Rijke tube can be represented by

$$u_f' = a_{01}^{(m)} + \sum_{l=1}^{\infty} b_{1l/m}\cos(l\Omega t/m) + c_{1l/m}\sin(l\Omega t/m) \tag{20}$$

$$p_f' = a_{02}^{(m)} + \sum_{l=1}^{\infty} b_{2l/m}\cos(l\Omega t/m) + c_{2l/m}\sin(l\Omega t/m) \tag{21}$$

where

$$
\begin{aligned}
a_{01}^{(m)} &= \frac{1}{L}\sum_{s=0}^{mL-1} u_f^{'}(t_s) \\
b_{1l/m} &= \frac{2}{L}\sum_{s=0}^{mL-1} u_f^{'}(t_s)\cos(l\Omega t_s / m) \\
c_{1l/m} &= \frac{2}{L}\sum_{s=0}^{mL-1} u_f^{'}(t_s)\sin(l\Omega t_s / m) \\
a_{02}^{(m)} &= \frac{1}{L}\sum_{s=0}^{mL-1} p_f^{'}(t_s) \\
b_{2l/m} &= \frac{2}{L}\sum_{s=0}^{mL-1} p_f^{'}(t_s)\cos(l\Omega t_s / m) \\
c_{2l/m} &= \frac{2}{L}\sum_{s=0}^{mL-1} p_f^{'}(t_s)\sin(l\Omega t_s / m)
\end{aligned}
\tag{22}
$$

The amplitude for the lth order of harmonic for the velocity and pressure at the position of heater then can be calculated as

$$
A_{l/m}^{(1)} = \sqrt{b_{1l/m}^2 + c_{1l/m}^2} \quad \text{and} \quad A_{l/m}^{(2)} = \sqrt{b_{2l/m}^2 + c_{2l/m}^2} \tag{23}
$$

3. Simulation and Discussions

In this section, the specific system parameters are chosen, which are tabulated in Table 1. In the simulation, only the first mode shape for the velocity and pressure is included, and the frequency of the excitation is assumed as Ω = 1.2. Figure 1 gives the bifurcation diagram of velocity and pressure at the heater for such as horizontal Rijke tube by varying the amplitude of excitation from 0 to 4. The steady-state response is periodic and the period is one period of excitation when the amplitude of excitation is greater than 1.736. The steady-state response suddenly becomes chaotic as the amplitude of excitation continues to decrease. In order to understand how chaotic motion for such a Rijke tube model forms as the amplitude of excitation decreases, the zoomed plots for velocity and pressure are illustrated in Figs.1(c) and (d). It can be found that the period-1 motion jumps to another period-17 motion at Ω = 1.736, and then it becomes chaotic at Ω = 1.72.

Table 1 System parameters for Horizontal Rijke Tube

Parameter Symbol	Value
c_1	0.1
c_2	0.06

x_f	0.3
τ	0.2
K	0.6
γ	1.4
M	0.6

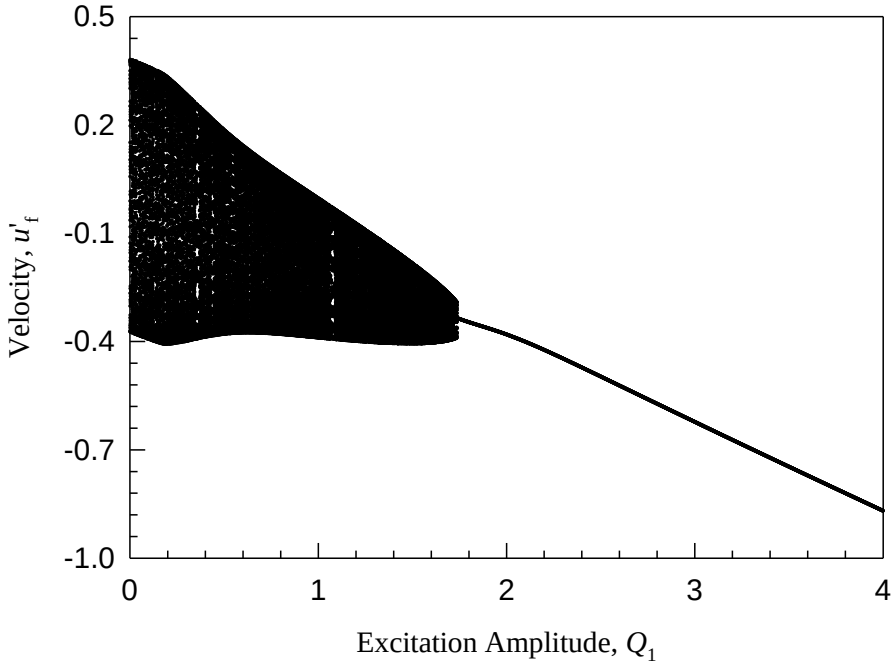

(a)

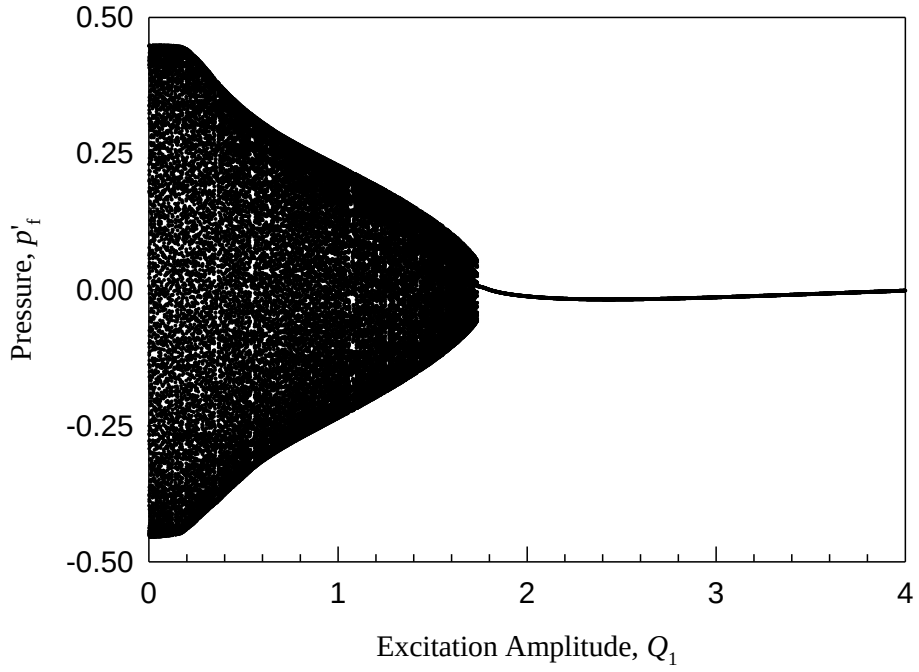

(b)

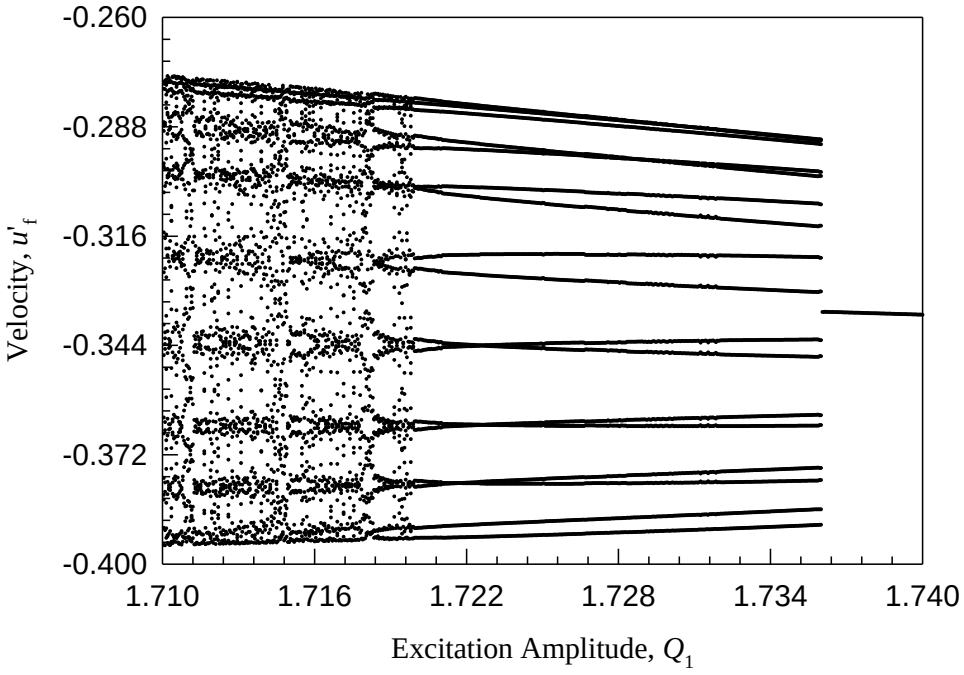

(c)

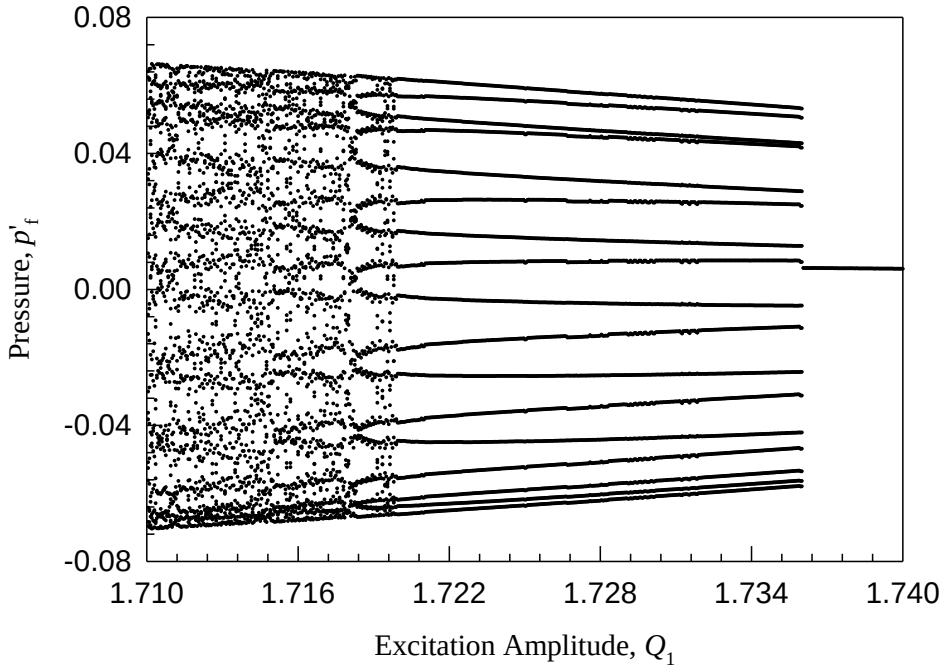

(d)

Fig. 1 Bifurcation for Rijke tube by varying excitation amplitude Q_1: (a) velocity at the heater, (b) pressure at the heater, (c) zoomed plot for velocity and (d) zoomed plot for pressure.

In Fig.2, the plots of node points of velocity and pressure at the heater varying excitation amplitude at the phase t = 0, $2\pi/\Omega$, $4\pi/\Omega$ … which are obtained by discrete implicit maps method are shown. The analytic solution of period-1 motion exists in the range of Q_1 = [0, 4]. The harmonic amplitudes of velocity and pressure for period-1 motions varying excitation amplitude are demonstrated in Figs.3 and 4, respectively. For harmonic amplitude of velocity

which is shown in Fig.3, the constant term is non-zero which indicates that average value of velocity oscillation is not zero for Q_1 = [0, 4]. It increases from zero at first, and then it drops around Q_1 = 1.8. The first order of harmonic increases almost linearly as the amplitude of excitation increases. For the higher harmonics, the quantity levels of $A_2^{(1)}$ and $A_3^{(1)}$ are both 10^{-2}, and the amplitude is almost zero when the excitation amplitude is small. When the order continues to increase, the range for which the harmonic amplitude is close to zero increases. For harmonic order increases to 10, the quantity level of harmonic amplitude decreases to 10^{-4}. The quantity level of harmonic amplitude of pressure also drops asymptotically with the order of harmonic increases which is illustrated in Fig.4. But for constant term of pressure at the heater, a_{02} is always zero.

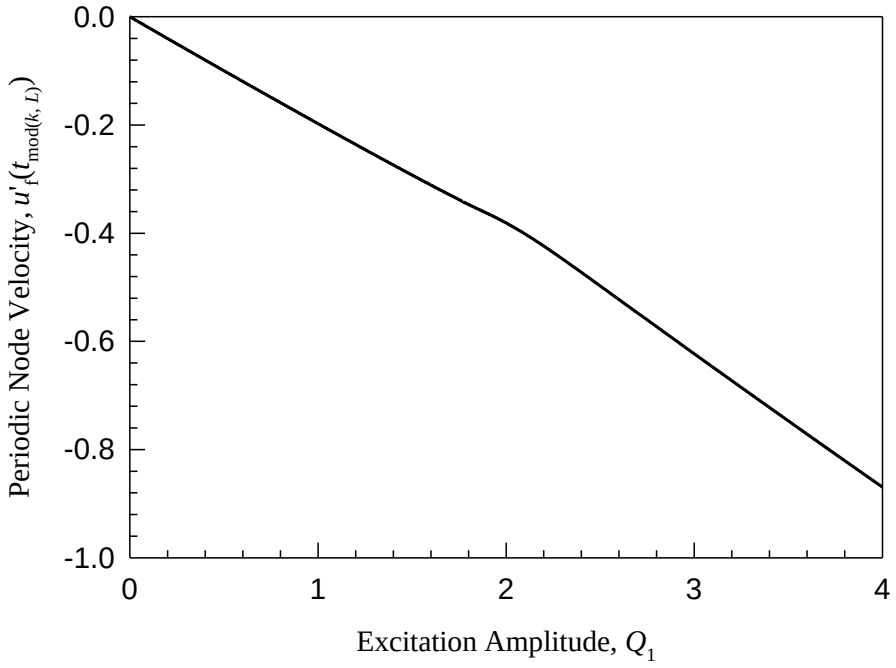

(a)

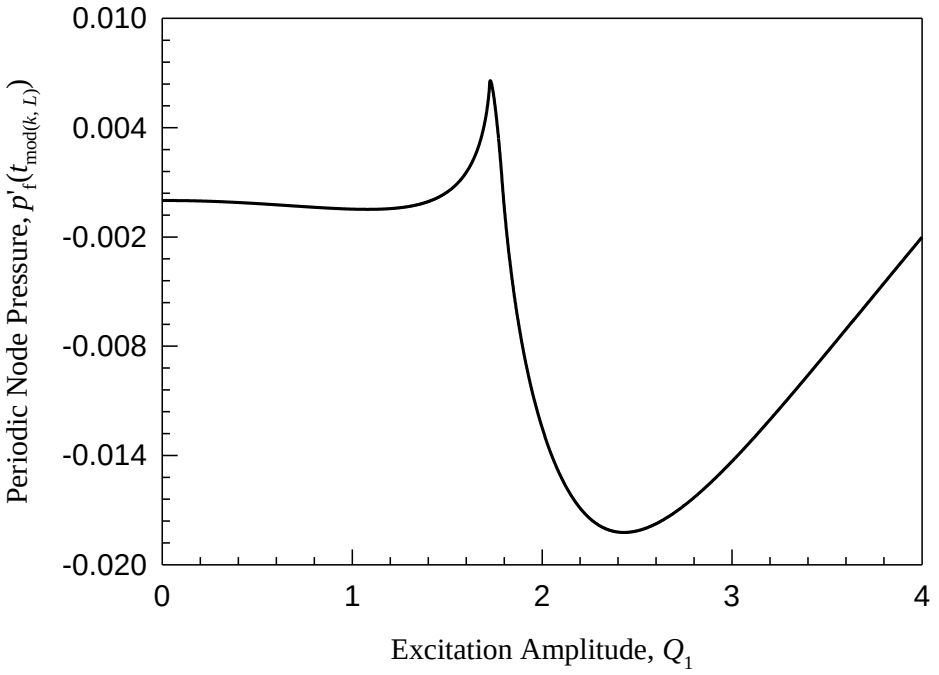

(b)

Fig. 2 Node points of period-1 motion at phase $t = t_{mod(k, L)}$ (k = 0, 1, 2…) varying excitation amplitude Q_1: (a) velocity at the heater, (b) pressure at the heater.

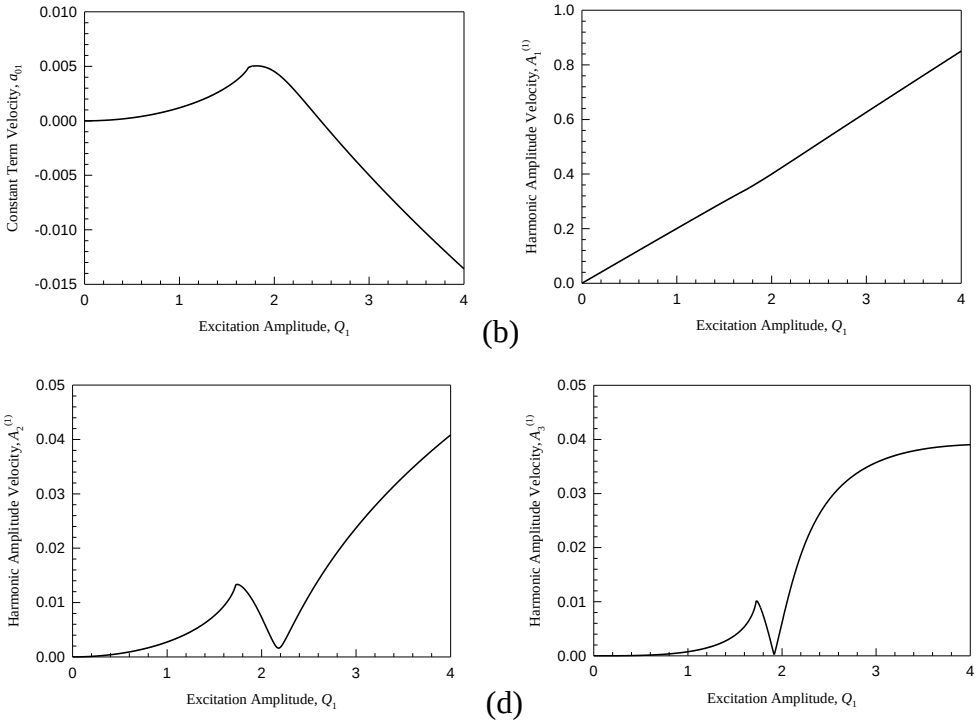

(a) (b)

(c) (d)

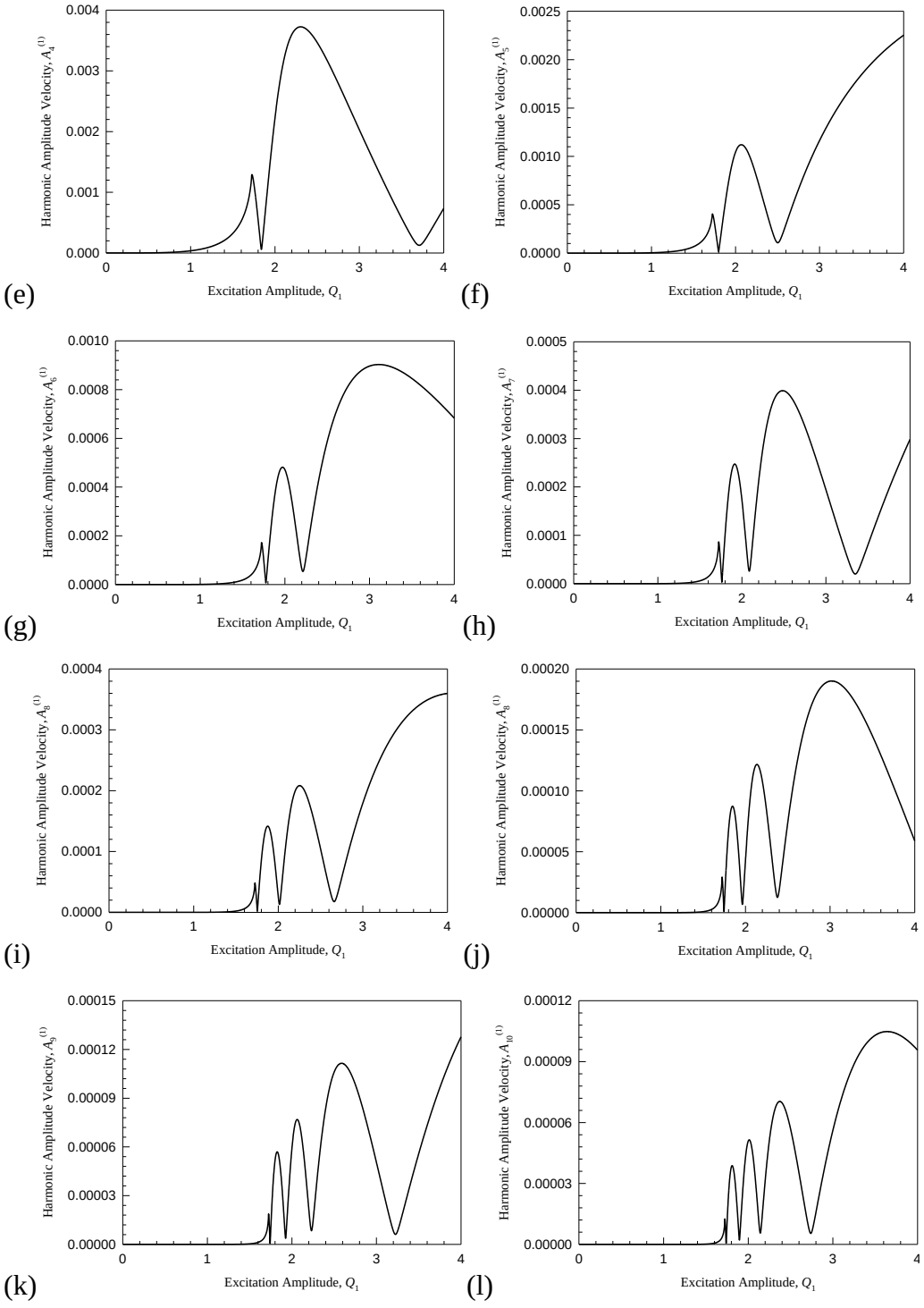

Fig. 3 Harmonic amplitude varying excitation amplitude Q_1 for velocity at heater: (a) constant term a_{01}, (b)-(l) $A_k^{(1)}$ (k = 1, 2,…, 10).

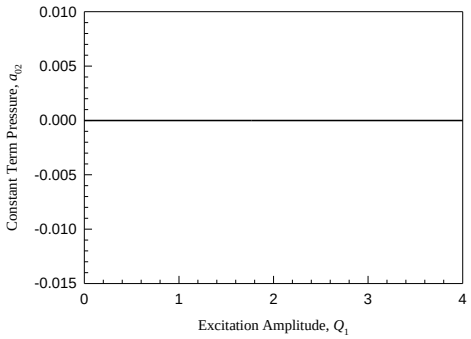
Constant Term Pressure, a_{02}
0.010
0.005
0.000
-0.005
-0.010
-0.015
0
1
2
3
4
Excitation Amplitude, Q_1

(a)

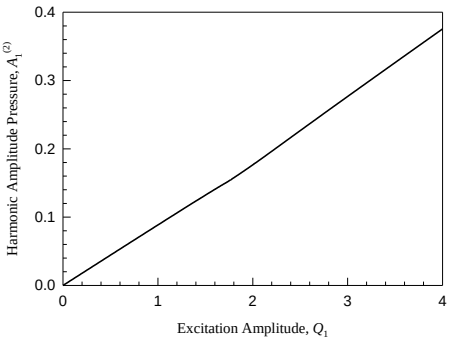
Harmonic Amplitude Pressure, $A_1^{(2)}$
0.4
0.3
0.2
0.1
0.0
0
1
2
3
4
Excitation Amplitude, Q_1

(b)

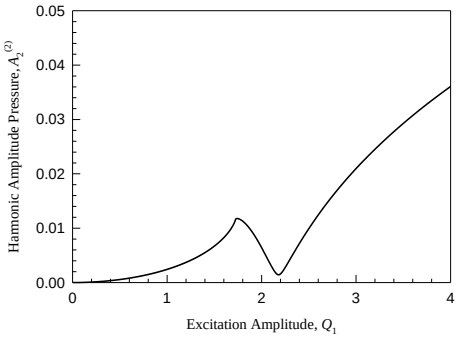
Harmonic Amplitude Pressure, $A_2^{(2)}$
0.05
0.04
0.03
0.02
0.01
0.00
0
1
2
3
4
Excitation Amplitude, Q_1

(c)

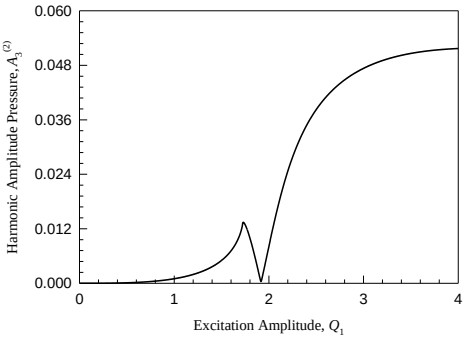
Harmonic Amplitude Pressure, $A_3^{(2)}$
0.060
0.048
0.036
0.024
0.012
0.000
0
1
2
3
4
Excitation Amplitude, Q_1

(d)

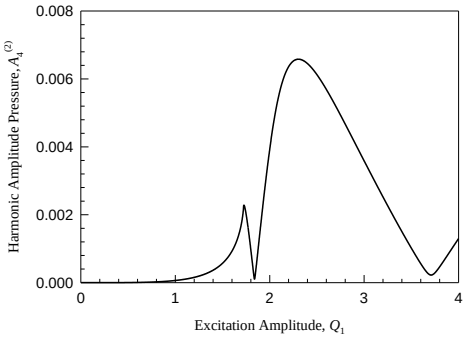
Harmonic Amplitude Pressure, $A_4^{(2)}$
0.008
0.006
0.004
0.002
0.000
0
1
2
3
4
Excitation Amplitude, Q_1

(e)

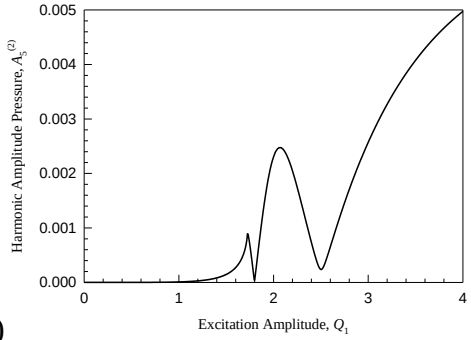
Harmonic Amplitude Pressure, $A_5^{(2)}$
0.005
0.004
0.003
0.002
0.001
0.000
0
1
2
3
4
Excitation Amplitude, Q_1

(f)

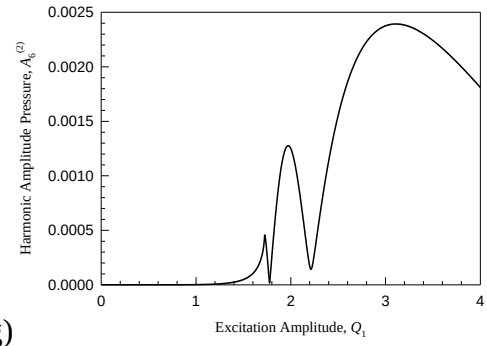
Harmonic Amplitude Pressure, $A_6^{(2)}$
0.0025
0.0020
0.0015
0.0010
0.0005
0.0000
0
1
2
3
4
Excitation Amplitude, Q_1

(g)

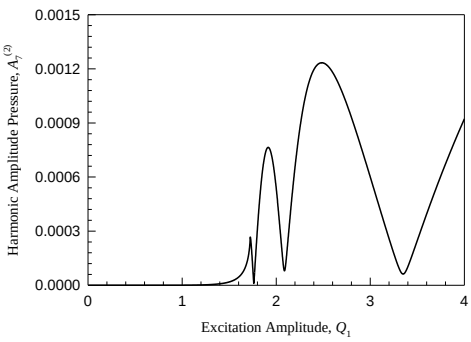
Harmonic Amplitude Pressure, $A_7^{(2)}$
0.0015
0.0012
0.0009
0.0006
0.0003
0.0000
0
1
2
3
4
Excitation Amplitude, Q_1

(h)

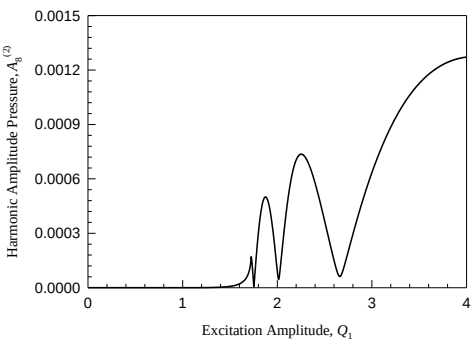
Harmonic Amplitude Pressure, $A_9^{(2)}$
0.0015
0.0012
0.0009
0.0006
0.0003
0.0000
0
1
2
3
4
Excitation Amplitude, Q_1

(i)

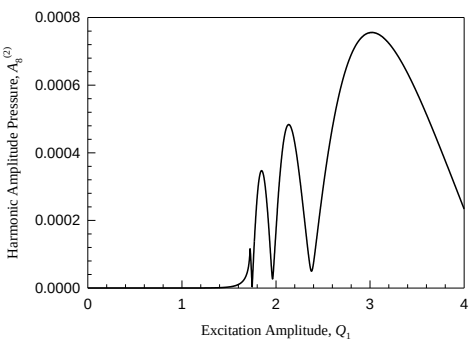
Harmonic Amplitude Pressure, $A_8^{(2)}$
0.0008
0.0006
0.0004
0.0002
0.0000
0
1
2
3
4
Excitation Amplitude, Q_1

(j)

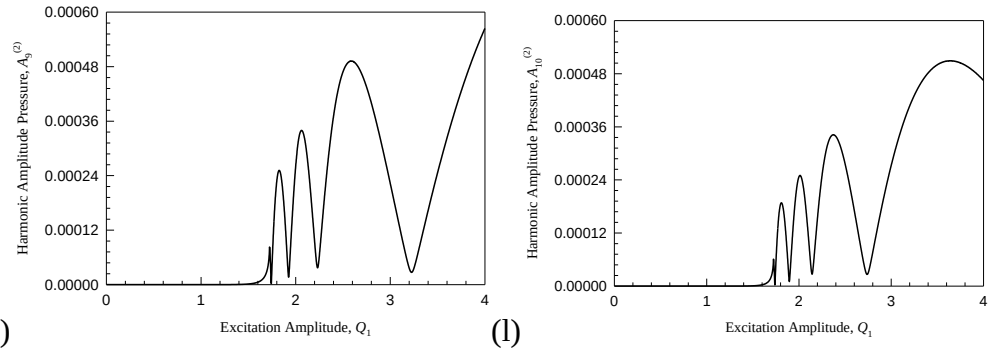

(k) (l)

Fig. 4 Harmonic amplitude varying excitation amplitude Q_1 for pressure at heater: (a) constant term a_{02}, (b)-(l) $A_k^{(2)}$ (k = 1, 2,…, 10).

For the analytical solution $\mathbf{z}$ which is obtained from discrete implicit maps method, the numerical simulation can be carried out with initial conditions from the analytical solution $\mathbf{z}$ of period-1 motion for Rijke tube. For the numerical simulation with Q_1 = 1.73 which is shown in Fig.5, the initial velocity and pressure at the heater are chosen as $u_f^{'} = -0.334259$, $p_f^{'} = 0.00653288$, respectively. In the phase plane, the solid curve is the numerical simulation. The green filled circle is the initial position, and the blue hollow circles are the time delayed information before t = 0. The red fork symbols are the analytical solution. For the first 20 periods, the trajectory from numerical simulation sticks to analytical solution of period-1 motion which is plotted in Figs.5(a)-(c). From Fig.1, the steady-state response for Q_1 = 1.73 is a period-17 motion. In order to investigate how motion involves from period-1 motion to period-17 motion, the Poincare maps of numerical simulation for Q_1 = 1.73 from 0 to 100 periods, from 100 to 200 periods, and from 300 to 400 periods are drawn in Figs.5(d)-(g), respectively. It can be seen that the motion sticks on the orbit of period-1 solution for the first 100 periods, and then it gradually leaves that orbit. After hundreds of periods of transient process, it runs to the stable period-17 orbit after 300 periods of simulation time.

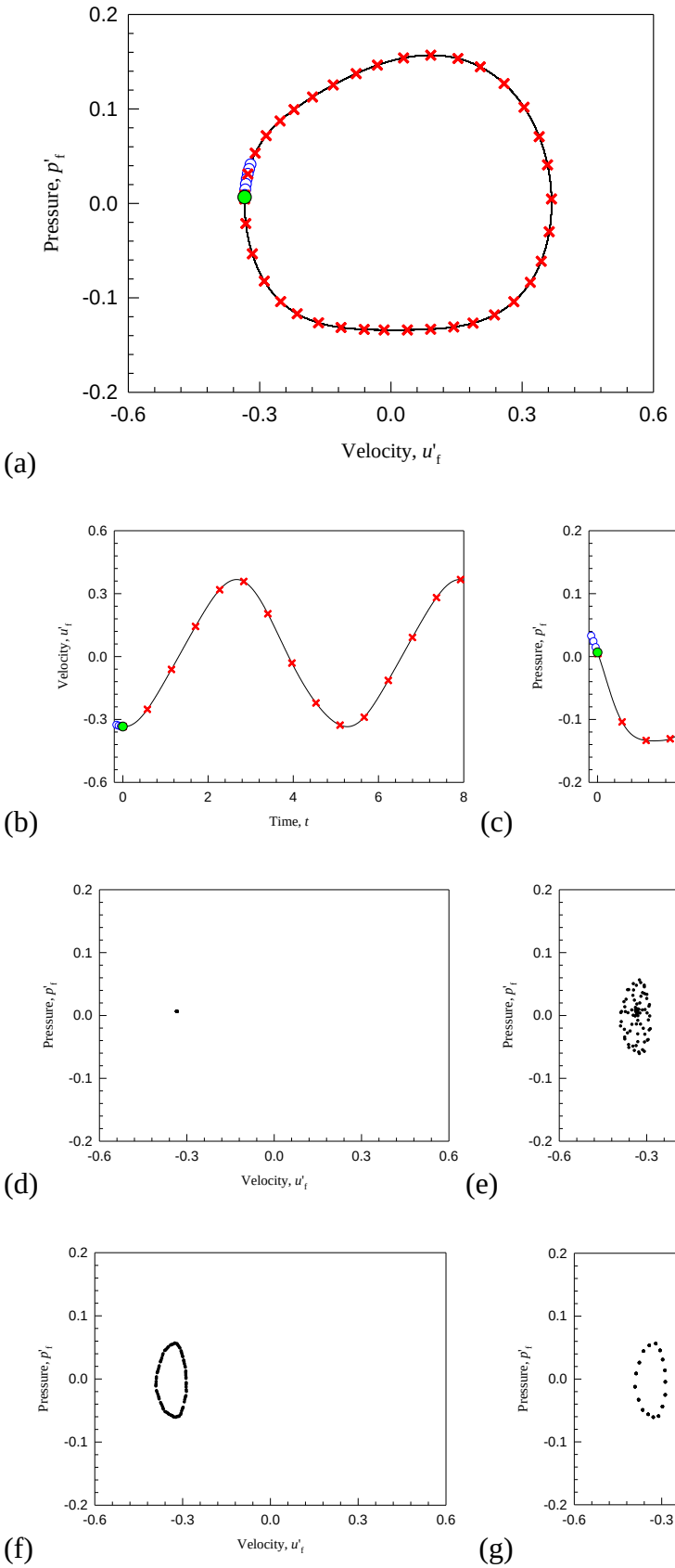

Fig. 5 Numerical simulation for Q_1 = 1.73 (u'_f = -0.334259, p'_f = 0.00653288 at t = 0): (a) phase plane, (b) time trajectory of velocity, (c) time trajectory of pressure for the first 20 periods; (d) Poincare map for 0 – 100 periods, (e) Poincare map for 100 – 200 periods (f) Poincare map for 200 – 300 periods, (g) Poincare map for 300 – 400 periods.

For Q_1 = 2.00, the stable period-1 motion is simulated with initial velocity and pressure at the heater $u_f^{'}$ = -0.380952 , $p_f^{'}$ = -0.0124891 , which is demonstrated in Fig.6. The numerical simulation correlates with the analytical solution very well, and it never leaves such an orbit. In Figs.6(d) and (e), the harmonic amplitudes of velocity and pressure are shown. The quantity level of harmonic amplitude of velocity drops to 10^{-6} when the order increases to 20. But the harmonic amplitude of pressure drops slower as the order of harmonic increases, and quantity level still stays around 10^{-6} as $k \rightarrow 50$.

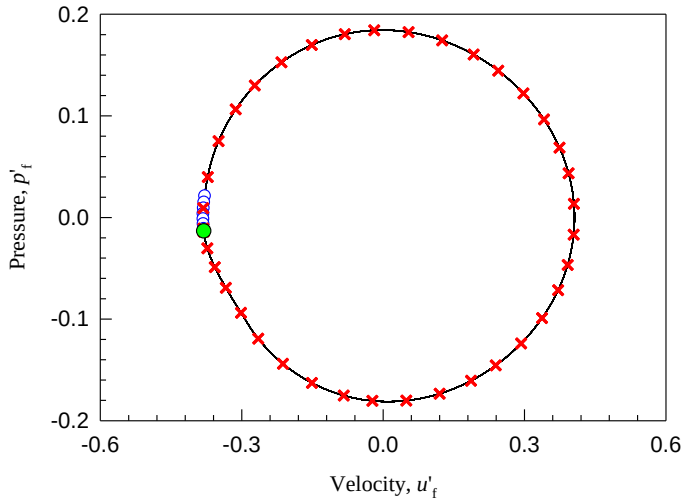

(a)

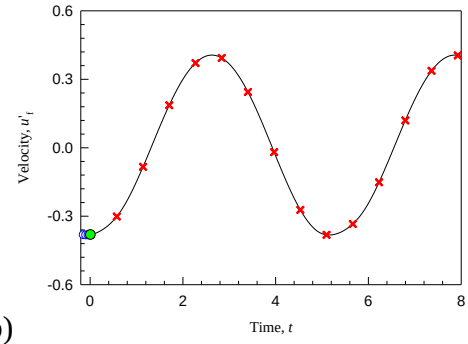

(b)

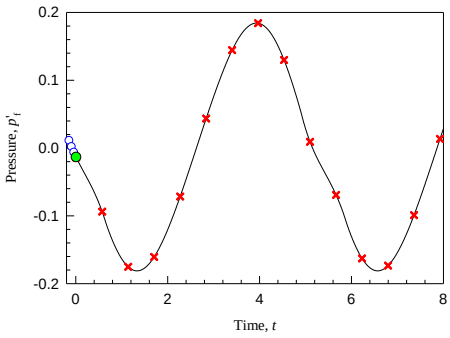

(c)

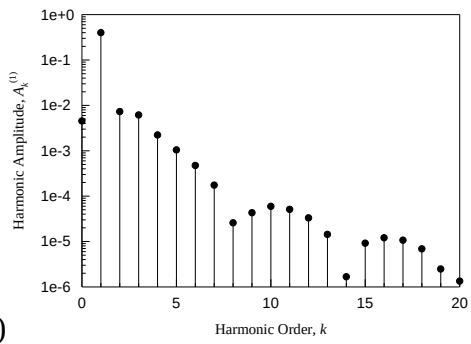

(d)

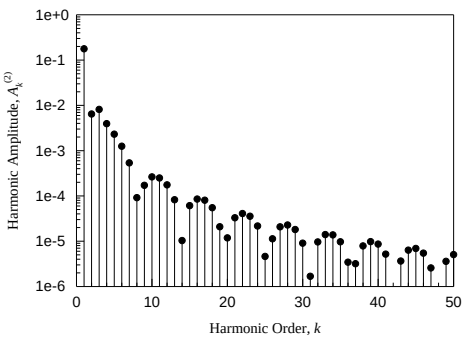

(e)

Fig. 6 Numerical simulation for Q_1 = 2.00 ($u_f^{'}$ = -0.380952, $p_f^{'}$ = -0.0124891 at t = 0): (a) phase plane, (b) time trajectory of velocity, (c) time trajectory of pressure, (d) harmonic amplitudes of velocity, (e) harmonic amplitudes of pressure.

4. Conclusions and future work

In this paper, the analytic solution of periodic motion for a horizontal Rijke tube model with periodic excitation has been obtained through discrete implicit approach. The procedures to discretizing the periodic motions and solving for the analytic solutions have been described in details. The analytic solutions of period-1 motion varying excitation amplitude have been presented. It shows that the solution of period-1 motion is continuously exists in the range of Q_1 = [0, 4], and no coexisting solution has been found in such a range. But for numerical bifurcation, it is known that period-1 motion disappears when the excitation amplitude continues to decrease at the critical point Q_1 = 1.736. By carrying out numerical simulation at Q_1 = 1.73 and 2.00, both the analytic solution before and after such a critical point should be exact, since the numerical prediction with initial conditions computed from the analytic solution of period-1 motion correlate with the analytic solution very well for the first many periods. For Q_1 = 2.00, the motion always sticks to the period-1 orbit. By observing the motion involving process using the Poincare map, it can be found that the motion stick with the analytic solution of period-1 motion for the first 100 periods, and then it runs to the orbit of perid-17 motion after 300 periods. It might be because the analytic solution of period-1 motion for such a horizontal Rijke tube is unstable for Q_1 < 1.736. Therefore, one have to continue to find out the way to determining the stability of periodic motion for such a Rijke tube which time-delay terms are included in the model in the future.

Acknowledgements

This work was sponsored by Shanghai Sailing Program (Grant No. 19YF1421600).

References

[1] Rijke, P.L. LXXI, "Notice of a new method of causing a vibration of the air contained in a tube open at both ends," Philosophical Magazine, 17(116), pp: 419-422, 1859.

[2] Rayleigh, "The explanation of certain acoustic phenomena," Nature, 18, pp: 319-321, 1878.

[3] Friedlander, M.M., Smith, T.J.B., Powell, A., "Experiments on the Rijke-tube phenomenon," The Journal of the Acoustical Society of America, 36(9), pp: 1737-1738, 1964.

[4] Bisio, G., Rubatto, G., "Sondhauss and Rijke oscillations-thermodynamic analysis, possible applications and analogies," Energy, 24(2), pp: 117-131, 1999.

[5] Balasubramanian, K., Sujith, R.I., "Thermoacoustic instability in a Rijke tube: Non-normality and nonlinearity," Physics of Fluids, 20(4), pp: 044103, 2008.

[6] Subramanian, P., Mariappan, S., Sujith, S., Wahi, P., "Bifurcation analysis of thermoacousitic instability in a horizontal Rijke tube," International Journal of Spray and Combustion Dynamics, 2(4), pp: 325-356, 2010.

[7] Mariappan, S., Sujith, R.I., "Modelling nonlinear thermoacoustic instability in an electrically heated Rijke tube," Journal of Fluid Mechanics, 680, pp: 511-533, 2011.

[8] Orchini, A., Rigas, G., Juniper, M.P., "Weakly nonlinear analysis of thermoacoustic bifurcations in the Rijke tube," Journal of Fluid Mechanics, 805, pp: 523-550, 2016.

[9] Huang, J.Z., Luo, A.C.J., "Periodic motions and bifurcation trees in a buckled, nonlinear Jeffcott rotor system," International Journal of Bifurcation and Chaos, 25(1), pp: 1550002, 2015.

[10] Luo, A.C.J., Jin, H.X., "Period-m motions to chaos in a periodically forced, Duffing oscillator with a time-delayed displacement," International Journal of Bifurcation and Chaos, 24(10), pp: 1450126, 2014.

[11] Yu, B., Luo, A.C.J., "Periodic motions and limit cycles of linear cable galloping," International Journal of Dynamics and Control, 6, pp: 41-78, 2018.

[12] Luo, A.C.J. Discretization and Implicit Mapping Dynamics. Springer, Berlin (2015).

[13] Wang, D.H., Huang, J.Z., "Periodic motions and chaos for a damped mobile piston system in a high pressure gas cylinder with P control," Chaos, Solitons & Fractals, 95, pp: 168-178, 2016.

[14] Guo, Y., Luo, A.C.J. Luo, "Complete bifurcation trees of a parametrically driving pendulum," Journal of Vibration Testing and System Dynamics, 1(2), pp: 93-134, 2017.

[15] Luo, A.C.J., Xing, S.Y., "Time-delay effects on periodic motions in a periodically forced, time-delayed, hardening Duffing oscillator," Journal of Vibration Testing and System Dynamics, 1(1), pp: 73-91, 2017.

[16] Matveev, K. I., Culick, F.E.C., "A Model for combustion instability involving vortex shedding," Combustion Science and Technology, 175(6), pp: 1059-1083, 2003.